Published in final edited form as:
Matrix Biol. 2012 May ; 31(4): 246–252. doi:10.1016/j.matbio.2012.02.004.

Connective Tissue Mineralization in *Abcc6*$^{-/-}$ Mice, a Model for Pseudoxanthoma Elasticum

N. Beril Kavukcuoglu[a,*], **Qiaoli Li**[b,*], **Nancy Pleshko**[a], and **Jouni Uitto**[b]

[a]Department of Bioengineering, Temple University, Philadelphia, PA 19122

[b]Department of Dermatology and Cutaneous Biology, Jefferson Medical College, Thomas Jefferson University, Philadelphia, PA 19107

Abstract

Pseudoxanthoma elasticum (PXE) is a heritable multisystem disorder characterized by ectopic mineralization. However, the structure of the mineral deposits, their interactions with the connective tissue matrix, and the details of the progressive maturation of the mineral crystals are currently unknown. In this study, we examined the mineralization processes in *Abcc6*$^{-/-}$ mice, a model system for PXE, by energy dispersive X-ray, and Fourier transform infrared imaging spectroscopy (FT-IRIS). The results indicated that the principal components of the mineral deposits were calcium and phosphate which co-localized within the histologically demonstrable lesions determined by topographic mapping. The Ca/P ratio increased in samples with progressive mineralization reaching the value comparable to that in endochondral bone. A progressive increase in mineralization was also reflected by increased mineral-to-matrix ratio determined by FT-IRIS. Determination of the mineral phases by FT-IRIS suggested progressive maturation of the mineral deposits from amorphous calcium phosphate to hydroxyapatite. These results provide critical information of the mechanisms of mineralization in PXE, with potential pharmacologic implications.

Keywords

Pseudoxanthoma elasticum; ectopic connective tissue mineralization; mineral composition; hydroxyapatite; FT-IRIS; treatment of mineralization disorders

1. Introduction

Pseudoxanthoma elasticum (PXE) is a heritable multisystem disorder, with clinical manifestations primarily in the skin, the eyes, and the cardiovascular system (Neldner, 1988). This disorder, caused by mutations in the *ABCC6* gene encoding a putative transmembrane transporter expressed primarily in the liver and the kidneys, shows clinically considerable, both intra- and interfamilial heterogeneity. The mode of inheritance is autosomal recessive with complete penetrance, but the clinical manifestations are of late-

Address for Correspondence: Jouni Uitto, MD, PhD, Department of Dermatology and Cutaneous Biology, Jefferson Medical College, 233 South 10th Street, Suite 450 BLSB, Philadelphia, PA 19107, Tel.: 215.503.5785, jouni.uitto@jefferson.edu.
*These authors contributed equally to this study.

onset, yet progressive, causing considerable morbidity and occasional mortality (Uitto et al., 2010).

The primary cutaneous lesions in PXE are yellowish papules on the sites of predilection, *i.e.*, on the side of the neck, antecubital fossae as well as the inguinal and periumbilical areas, which progressively coalesce into larger inelastic plaques of leathery and inelastic skin. The cutaneous findings are primarily of cosmetic concern, but they signify the potential of serious ocular and cardiovascular complications. Specifically, the eye findings manifest with early angioid streaks due to breaks in Bruch's membrane, an elastin rich sheath behind the retinal pigmented epithelium, which lead to choroidal neovascularization, hemorrhage, and scarring manifesting with progressive loss of visual acquity and blindness. The cardiovascular manifestations include hypertension, intermittent claudication, rupture and bleeding of blood vessels within the gastrointestinal tract, and rarely, early myocardial infarcts and strokes (Georgalas et al., 2011; Mendelsohn et al., 1978; Neldner, 1988).

Histopathology of the cutaneous lesions demonstrates accumulation of pleiomorphic elastic structures which become progressively mineralized early on, while at later stages mineralization of collagen matrix is also noted by transmission electron microscopy (Klement et al., 2005). The ocular manifestations are associated with mineralization of Bruch's membrane, and a characteristic pathologic feature in the cardiovascular system is mineralization of the arterial blood vessels. Histopathologic examination of the affected tissues with special stains, such as Alizarin Red and von Kossa stains, has suggested that the mineral deposits consist of calcium phosphate complexes. However, the mechanisms of mineralization as well as the initiating factors are largely unknown (Uitto et al., 2011). Furthermore, the structure of the mineral deposits, their interactions with the connective tissue matrix, and the details of the progressive maturation of the mineral crystals are currently unknown.

In general, mineral compounds deposited during either physiologic or pathologic mineralization have distinct spectral features, which provide a fingerprint of the compounds present. Both Fourier transform infrared (FTIR) and Raman spectroscopy, techniques based on molecular vibrations, have been used to gain information on the nature of mineral phases, and the relative amount of these phases with respect to the organic matrix (Boskey and Pleshko Camacho, 2007; Boskey and Mendelsohn, 2005; Camacho et al., 2003; Kavukcuoglu et al., 2007; Kavukcuoglu et al., 2009; Pleshko et al., 1991). FTIR infrared imaging spectroscopy (FT-IRIS), a modality in which the FTIR spectrometer is coupled to a light microscope and an array detector, can be used to collect data from an entire histological section of tissue sample with 6.25 μm pixel resolution. This method provides information on the identity of the mineral phase as well as the relative amount and spatial distribution of mineral present (Sauer et al., 1988, 1994; Wentrup-Byrne et al., 1997). This technique also provides advantages in detecting small changes in relatively large and inhomogeneous structures with high speed and resolution. In addition, for pathological mineralizations where more than one phase is present, FT-IRIS has been proposed to be the most rapid way of locally identifying the phases (Boskey and Mendelsohn, 2005).

Several studies have utilized infrared spectroscopy and microscopy to evaluate pathological mineralization in different clinical settings. Boskey and Mendelsohn utilized IR imaging to investigate the mineral phases associated with juvenile dermatomyositis and found deposition of hydroxyapatite (HA) in association with the lipid phase (Boskey and Mendelsohn, 2005). Other FTIR spectroscopy and imaging studies investigating pathological mineralizations have found the deposition of HA in calcinosis cutis (Liu et al., 2005), iron oxide deposits in thalassemia (Chua-anusorn and Webb, 2000), and HA deposits in atherosclerotic plaques (Manoharan et al., 1993) as well as in juvenile dermatomyositis

(Pachman and Boskey, 2006). An octacalcium phosphate-like (OCP-like) precursor phase was found to transform into HA deposits in prosthetic heart valves (Tomazic et al., 1994). In some cases more than one mineral phase was detected, and, for example, calcium oxalate, whitlockite, and HA deposits were evident in kidney and salivary stones, while calcium pyrophosphate dihydrate (brushite), monosodium urate, HA and calcium oxalate deposits were found in articular cartilage and intervertebral disk deposits (Boskey and Mendelsohn, 2005).

In the current study, we utilized FTIR imaging spectroscopy to identify mineral phases and to monitor progress of mineral deposition in the connective tissue capsule of the vibrissae, as well as in the heart and kidney tissues of *Abcc6*$^{-/-}$ mice, a model system recapitulating features of PXE.

2. Results

2.1 Progressive mineralization of connective tissues in Abcc6$^{-/-}$ mice

The *Abcc6*$^{-/-}$ (KO) mice were developed by targeted ablation of exons 15–18 through homologous recombination (Klement et al., 2005). Previous studies have demonstrated that these mice develop progressive mineralization which is first noted at ~5–6 weeks of age. The first site of mineralization is the connective tissue capsule surrounding the bulb of vibrissae in the muzzle skin, and this mineralization process has been shown to be progressive throughout the remaining life of these mice (Jiang et al., 2007). In addition to skin, mineralization has been previously shown to take place in the retina, arterial blood vessels, heart and kidneys (Klement et al., 2005). In this study, we first examined the degree of mineralization in 3, 6, and 24 month old mice, in comparison to wild-type littermates, utilizing the Alizarin red staining method. All mice had the same genetic background with 5 crosses into C57BL/6J.

Our histopathology results demonstrated that the mineralization of the connective tissue capsule surrounding the vibrissae in the skin was clearly detectable in mice at three months of age, and was more pronounced at 6 and 24 months (Fig. 1A–C). Similarly, distinct foci of mineralization were noted in blood vessels of the heart and kidneys at three months of age, and the overall degree of mineralization in these tissues was more extensive at 24 months (Fig. 1G,H). These observations confirm that, similar to patients with PXE, the mineralization process is progressive in the *Abcc6*$^{-/-}$ mice.

2.2 Demonstration that the mineral deposits consist predominantly of calcium and phosphate

The histopathologic studies demonstrating mineralization of connective tissues utilized Alizarin Red which recognizes calcium phosphate complexes. To physically identify the composition of the mineral deposits, energy dispersive X-ray (EDAX) analyses were performed on the connective tissue capsule of the vibrissae. The results demonstrated prominent peaks corresponding to calcium and phosphate (Fig. 2A). Topographic (RADAR) mapping demonstrated that calcium and phosphate co-localized with the histologically demonstrable mineral deposits, suggesting the presence of calcium phosphate complexes (Fig. 2B). Minor peaks were also noted corresponding to aluminum and ferrous iron, however, these signals did not co-localize with the mineral deposits, and were most likely derived from the metal carrier on which the sections were placed for analysis. Thus, these analyses, together with special stains, suggest that the mineral deposits consist of calcium phosphate complexes. We also quantitated the ratio of Ca/P from EDAX analysis at different stages of mineralization. As shown in Fig. 2C, this ratio progressively increased in

samples from mice between 3 and 24 months of age, reaching a value comparable to that in endochondral bone which has characteristic HA.

2.3 Identification and maturation of mineral deposits in Abcc6$^{-/-}$ mice

To identify the mineral phases and monitor their maturation, mineral deposits were examined by Fourier transform infrared imaging spectroscopy (FT-IRIS). Infrared absorbance bands associated with phosphate mineral vibrations (between 1200–900 cm^{-1}) were evident at the connective tissue capsule surrounding the vibrissae and heart blood vessels of the KO mice (Fig. 3). The spatial distribution of the mineralization in the vibrissae can be visualized for a set of representative samples in the FT-IRIS images of the mineral to matrix ratio (Fig. 1D–F). These images are consistent with the histological results that also showed mineral deposits on the connective tissue capsule surrounding the bulb of vibrissae. A progressive increase in mineralization in the vibrissae during aging of the PXE mouse model was also evident based on the mineral-to-matrix (organic) ratio from 3 to 24 months (Fig. 4A). The crystallinity, an indicator of mineral maturity, was shown to increase from 3 months to 6 months and remained the same for 24 month old sample (Fig. 4B). These data did not reach statistical significance due to the small number of samples.

Identification of the mineral phases was based on infrared spectra from standard biological calcium phosphate compounds, including amorphous calcium phosphate (ACP), and hydroxyapatite (HA). In general, ACP phases have broad, featureless infrared absorbance bands, while more crystalline phases display sharper, more defined peaks (Pleshko et al., 1991). Three out of seven muzzle skin samples from the 3 month old mice did not have detectable mineral peaks. In those tissues where mineralization was evident, the predominant phase was ACP (Fig. 5A). The 6 month old samples generally displayed more defined peaks with a strong absorbance at 1024 cm^{-1} in the phosphate region, which is attributable to poorly crystalline HA (Fig. 5B). There was also a peak at 876 cm^{-1} , likely associated with the $\nu 2$ CO_3 bending mode of carbonate incorporated into hydroxyapatite. However, there were also some regions of mineralization in the 6 month samples that showed spectra consistent with ACP. The spectra obtained from the 24 month old samples had evidence of some ACP (spectra not shown) but was primarily a poorly crystalline HA, as evidenced by the peaks at ~1024 and 876 cm^{-1} (Fig. 5C). The heart and kidneys of *Abcc6*$^{-/-}$ mice did not have as extensive a mineralized region as the vibrissae samples. Among the heart samples, only some were shown to have detectable mineral deposition. The majority of the mineral phase was ACP, but in small regions poorly crystalline HA was also observed with very low absorbance levels (Fig. 5D). Unlike the heart samples, there was no evidence of an apatitic phase in kidney samples, and only one sample had evidence of ACP (Fig. 5E).

3. Discussion

Characterization of the temporal progression of pathological mineralization in PXE could provide an opportunity for disease intervention. In the current study, the nature of the ectopic mineral phase in multiple organs from the *Abcc6*$^{-/-}$ mouse model of PXE was examined and found to be complex and non-uniform. Pathological or ectopic tissue mineralization, unlike the physiological mineralization of bone, is an uncontrolled process that occurs in soft connective tissues due to genetic, inflammatory, or metabolic disorders, as well as in joint cartilage as a result of degenerative joint disease. It is not uncommon for several calcium phosphate phases to occur together during these processes (Elliott, 2002).

In the current study we analyzed the mineral content and composition of tissues in *Abcc6*$^{-/-}$ mice, a model system for PXE, a heritable connective tissue mineralization disorder. In this mouse model, similar to patients with PXE, mineralization has been demonstrated in the

skin, blood vessels, and other tissues by histopathologic staining using von Kossa or Alizarin Red techniques (Neldner, 1988; Klement et al., 2005). These histopathologic observations were confirmed by EDAX analyses which demonstrated prominence of calcium and phosphate in the mineral deposits, and the ratio of these ions in fully matured lesions was similar to that noted in endochondral bone.

Identification of the mineral phases by FT-IRIS indicated the presence of ACP in the connective tissue capsule of vibrissae of 3 month old KO mice, as evidenced by the broad and featureless absorbance band. ACP has been seen as a precursor phase in the biomineralization process (Johnsson and Nancollas, 1992; Mahamid et al., 2008), and thus it is likely that ACP would be converted to a crystalline phase over time. In contrast to the broad, amorphous spectra found in tissues of 3 month old mice, samples from the 6 month old KO mice showed the presence of HA, a poorly crystalline mineral phase, based on the appearance of a narrower peak at 1024 cm^{-1} and an absorbance band centered at 876 cm^{-1}. In the spectral range of interest, biological HA displays a broad contour in the 900 – 1200 cm^{-1} range, with band narrowing evident at 960 cm^{-1} (symmetric phosphate stretch), and ~ 1025 cm^{-1} (phosphate asymmetric stretch), a shoulder near ~ 1110 cm^{-1} (possibly due to acid phosphate), and a smaller absorbance from carbonate substitution in the apatite, centered at ~ 870 cm^{-1} (Pleshko et al., 1991).

Similar to the mineralization phases noted in the 6 month samples, the 24 month old tissues also contained poorly crystalline HA in most of the mineralized regions, based on the distinct phosphate band at ~1024 cm^{-1} attributable to the phosphate $\nu 1$ and $\nu 3$ vibrations, and the carbonate band at 876 cm^{-1}, mixed with ACP. Thus, ACP was found in the vibrissae at all ages and the HA phase was only found at 6 and 24 months of age. Further, a trend towards increased mineralization and HA crystallinity occurred with aging in the mice. Together, these data suggest that the initial mineral phase nucleated is ACP and that this continues to be formed, even through two years of age. Further, poorly crystalline HA deposits mature during aging, and also increase in quantity.

Low levels of mineralization were found in the heart and kidneys, primarily associated with the blood vessels in these organs. The ability of elastin to serve as a nucleation site for mineralization is consistent with the observation that in the skin of patients with PXE, there is an accumulation of pleiomorphic elastotic material, the primary site of mineralization (Neldner, 1988). Also, in *Abcc6*$^{-/-}$ mice collagen fibers become mineralized at later stages (Klement et al., 2005). The precise mechanisms by which elastin or its degradation products might elicit mineralization are not well understood (Pai and Giachelli, 2010). However, collagen mineralization generally proceeds through bound non-collagenous phosphoproteins (Glimcher, 1989). These observations may have implications to the degree by which different organs are mineralized in *Abcc6*$^{-/-}$ mice. Specifically, mineralization of blood vessels, in comparison to connective tissue sheath of vibrissae, which contain both elastin and collagen (Klement et al., 2005), may be affected by the availability of elastic structures for nucleation as well as by tissue-specific micro-environment that favors mineralization, including the local concentrations of calcium and phosphate and the presence of local and systemic anti-mineralization factors (Jiang et al., 2007).

An alternate explanation relates to the possibility of matrix-vesicle nucleated mineralization. Matrix vesicles (MVs) have been shown to play an important role in both skeletal (Anderson and Reynolds, 1973) and ectopic mineralization (Derfus et al., 1992; Hsu and Camacho, 1999). Studies of the role of MVs in the deposit of brushite and HA during endochondral calcification have provided insight into the pathways of pathological mineralization (Thouverey et al., 2009). It has been suggested that pathological mineralization of soft tissues has a mechanism similar to skeletal calcification and that MVs may play a similar

role in both mechanisms (Golub, 2010), where they serve as nucleation sites. It was also shown that vascular calcification follows the known biomineralization pathway where MV or MV-like particles appear in the hard tissue modulating the local PO_4^{3-}/POP (inorganic pyrophosphate) ratio and providing sites for crystal nucleation (Golub, 2010). POP is a potent inhibitor for mineral formation, and changing the PO_4^{3-}/ POP ratio would trigger or inhibit mineral formation. Previously, FTIR imaging was used to identify mineral phases associated with MV-induced *in vitro* mineralization (Garimella et al., 2006). However currently, it is unknown whether MVs play a role in PXE-associated mineralization.

The results of this study suggest that prevention of PXE-associated mineralization could possibly be attained by inhibiting the formation of early precursors and their transformation into apatitic or other crystalline mineral phases. FT-IRIS data such as these can provide additional information on the mechanisms of mineralization caused by PXE and may play an important role in early diagnosis and the development and monitoring of treatment. In this context, it is of interest that feeding *Abcc6*$^{-/-}$ mice a diet enriched in Mg^{2+} (5×) beginning at 4 weeks of age completely prevented the mineralization of the connective capsule of vibrissae, *i.e.*, before the calcium phosphate deposition ensues (LaRusso, 2009; Li et al., 2009). However, feeding the mice a Mg^{2+}-enriched diet beginning at 3 months of age for 12 weeks failed to reverse the mineralization, although the amount of mineral deposits did not further increase. These observations would be consistent with a notion that macromolecular addition of Mg^{2+} prevents the early mineral deposition and growth while having little, if any, effect on fully mature HA crystals. Thus, Mg^{2+} enriched diet may provide a novel approach to ameliorate the mineralization in PXE, but it is essential to prevent mineral nucleation as soon as possible, and in patients with PXE such treatment should be initiated as soon as the definitive diagnosis has been established.

4. Experimental procedures

4.1 Development and characterization of Abcc6$^{-/-}$ mice

The *Abcc6*$^{-/-}$ mice *(Abcc6*^{tm1JfK}*)* were developed by targeted inactivation of the *Abcc6* gene (Klement et al., 2005). Both wild-type and knock-out mice on the C57BL/6J genetic background were maintained in the Animal Facility of Thomas Jefferson University and housed in a temperature and humidity controlled environment under 12-hour light/dark cycle. The mice were fed with a standard rodent diet (Lab Diet 5010; PMI Nutrition, Brentwood, MO, USA), and had free access to water. The animal studies were approved by the Institutional Animal Care and Use Committee of the Thomas Jefferson University.

Tissue specimens obtained from the mice at necropsy were fixed in formaldehyde and embedded in paraffin. Sections of 5 μm were prepared and subjected to histopathologic analysis by hematoxylin-eosin and Alizarin red stains. Sections containing mineral deposits were used for analysis by EDAX and FT-IRIS.

4.2 Energy dispersive X-ray analysis of elements composition

Paraffin sections of biopsies from muzzle skin containing vibrissae were mounted onto metal carriers and then coated with carbon using a sputter coater to increase conductivity. Specimens were imaged and analyzed for elemental composition in a JEOL-T330A scanning electron microscope (JEOL Ltd, Tokyo, Japan) fitted with an energy dispersal X-ray elemental analyzer. X-ray maps of coated samples were collected and topographic mapping of calcium and phosphate was analyzed by Noran System Six (Thermo Scientific) program.

4.3 Fourier transform infrared spectroscopy data collection and analysis

Vibrissae samples from 3 month (n=4), 6 month (n=7), and 24 month (n=3) old mice, heart samples from 24 month (n=5), and kidney samples from 24 month (n=2) old mice were investigated by FT-IRIS for identification of the mineral phases. Two consecutive sections were used for histology and FT-IRIS. The mineralized regions were first identified in histology slides and then FT-IRIS data collected in the corresponding region. Paraffin-embedded samples were sectioned at 6 μm thickness onto low-e slides (Kevley Technologies, OH) or BaF_2 windows for FT-IRIS imaging studies. Data were acquired in transflectance (low-e slides) or transmittance (BaF_2 windows) mode with a Perkin Elmer Spotlight 400 Imaging System (Perkin Elmer, Shelton, CT). All images were collected in the mid-IR range (2000–748cm^{-1}) at a spectral resolution of 8 cm^{-1} and pixel resolution of 6.25 μm.

Infrared images were created using ISys software V5.0 (Malvern Instruments, Columbia, MD). To identify the mineral phases present in the tissues, the mineral absorbance band contour and frequencies were compared to that of amorphous calcium phosphate (ACP) and hydroxyapatite (HA). The bands associated with the mineral vibrations of the $\nu 1, \nu 3$ phosphate (PO_4^{3-}) absorbance from 1200 to 900 cm^{-1} and the collagen related amide I (matrix) band at 1590–1720 cm^{-1} were investigated. Absorbances in this region are a result of vibrations associated with symmetric and asymmetric P-O bond stretching and carbonyl stretching bonds, respectively. Spectra were baselined and images created from the peak height ratio of the phosphate to amide I (mineral to matrix) to assess the extent of mineralization (Boskey and Pleshko Camacho, 2007; Camacho et al., 2003; Pleshko et al., 1991). In the current study, as the mineral observed was apatitic, the crystallinity was calculated as the ratio of the peak heights at 1030 cm^{-1} and 1020 cm^{-1} (data from BaF_2 samples only) which correlates linearly with the HA crystal size and perfection (Boskey and Mendelsohn, 2005). One way ANOVA was performed to assess differences among the FT-IRIS parameters of mineral-to-matrix ratio and crystallinity at different ages.

Highlights

- We examined the mineralization processes in *Abcc6*$^{-/-}$ mice, a model system for PXE, by energy dispersive X-ray, and Fourier transform infrared imaging spectroscopy (FT-IRIS).
- The principal components of the mineral deposits were calcium and phosphate.
- Determination of the mineral phases by FT-IRIS suggested progressive maturation of the mineral deposits from amorphous calcium phosphate to hydroxyapatite.
- These results provide critical information of the mechanisms of mineralization in PXE, with potential pharmacologic implications.

Acknowledgments

The authors wish to thank Carol Kelly (TJU) and Claire Ya-Ting Ou (TU) for technical assistance. This study was supported by NIH/NIAMS grants R01 AR28450 and R01 AR55225 (JU). QL is recipient of a Research Career Development Award from Dermatology Foundation.

Abbreviations

PXE pseudoxanthoma elasticum

KO	knockout
EDAX	energy dispersive X-ray
FT-IRIS	Fourier transform infrared imaging spectroscopy

References

Anderson HC, Reynolds JJ. Pyrophosphate stimulation of calcium uptake into cultured embryonic bones. Fine structure of matrix vesicles and their role in calcification. Dev. Biol. 1973; 34:211–227. [PubMed: 4363671]

Boskey A, Pleshko Camacho N. FT-IR imaging of native and tissue-engineered bone and cartilage. Biomaterials. 2007; 28:2465–2478. [PubMed: 17175021]

Boskey AL, Mendelsohn R. Infrared spectroscopic characterization of mineralized tissues. Vib. Spectrosc. 2005; 38:107–114. [PubMed: 16691288]

Camacho NP, Carroll P, Raggio CL. Fourier transform infrared imaging spectroscopy (FT-IRIS) of mineralization in bisphosphonate-treated oim/oim mice. Calcif. Tissue Int. 2003; 72:604–609. [PubMed: 12574874]

Chua-Anusorn W, Webb J. Infrared spectroscopic studies of nanoscale iron oxide deposits isolated from human thalassemic tissues. J. Inorg. Biochem. 2000; 79:303–309. [PubMed: 10830881]

Derfus BA, Rachow JW, Mandel NS, Boskey AL, Buday M, Kushnaryov VM, Ryan LM. Articular cartilage vesicles generate calcium pyrophosphate dihydrate-like crystals *in vitro*. Arthritis Rheum. 1992; 35:231–240. [PubMed: 1734912]

Elliott JC. Calcium phosphate biominerals. Rev. Mineral. Geochem. 2002:427–453.

Fowler BO, Moreno EC, Brown WE. Infra-red spectra of hydroxyapatite, octacalcium phosphate and pyrolysed octacalcium phosphate. Arch. Oral Biol. 1966; 11:477–492. [PubMed: 5226756]

Garimella R, Bi X, Anderson HC, Camacho NP. Nature of phosphate substrate as a major determinant of mineral type formed in matrix vesicle-mediated *in vitro* mineralization: An FTIR imaging study. Bone. 2006; 38:811–817. [PubMed: 16461032]

Georgalas I, Tservakis I, Papaconstaninou D, Kardara M, Koutsandrea C, Ladas I. Pseudoxanthoma elasticum, ocular manifestations, complications and treatment. Clin. Exp. Optom. 2011; 94:169–180. [PubMed: 21198842]

Glimcher MJ. Mechanism of calcification: role of collagen fibrils and collagen-phosphoprotein complexes *in vitro* and *in vivo*. Anat. Rec. 1989; 224:139–153. [PubMed: 2672881]

Golub EE. Biomineralization and matrix vesicles in biology and pathology. Semin. Immunopathol. 2010; 33:409–417. [PubMed: 21140263]

Hsu HH, Camacho NP. Isolation of calcifiable vesicles from human atherosclerotic aortas. Atherosclerosis. 1999; 143:353–362. [PubMed: 10217364]

Jiang Q, Li Q, Uitto J. Aberrant mineralization of connective tissues in a mouse model of pseudoxanthoma elasticum: Systemic and local regulatory factors. J. Invest. Dermatol. 2007; 127:1392–1402. [PubMed: 17273159]

Johnsson MS, Nancollas GH. The role of brushite and octacalcium phosphate in apatite formation. Crit. Rev. Oral Biol. Med. 1992; 3:61–82. [PubMed: 1730071]

Kavukcuoglu NB, Patterson-Buckendahl P, Mann AB. Effect of osteocalcin deficiency on the nanomechanics and chemistry of mouse bones. J. Mech. Behav. Biomed. Mater. 2009; 2:348–354. [PubMed: 19627841]

Klement JF, Matsuzaki Y, Jiang QJ, Terlizzi J, Choi HY, Fujimoto N, Li K, Pulkkinen L, Birk DE, Sundberg JP, Uitto J. Targeted ablation of the abcc6 gene results in ectopic mineralization of connective tissues. Mol. Cell Biol. 2005; 25:8299–8310. [PubMed: 16135817]

LaRusso J, Li Q, Jiang Q, Uitto J. Elevated dietary magnesium prevents connective tissue mineralization in a mouse model of pseudoxanthoma elasticum (Abcc6(−/−)). J. Invest. Dermatol. 2009; 129:1388–1394. [PubMed: 19122649]

Li Q, Larusso J, Grand-Pierre AE, Uitto J. Magnesium carbonate-containing phosphate binder prevents connective tissue mineralization in Abcc6(−/−) mice-potential for treatment of pseudoxanthoma elasticum. Clin. Transl. Sci. 2009; 2:398–404. [PubMed: 20443931]

Liu MT, Cheng WT, Li MJ, Liu HN, Yang DM, Lin SY. Identification of chemical compositions of skin calcified deposit by vibrational microspectroscopies. Arch. Dermatol. Res. 2005; 297:231–234. [PubMed: 16231145]

Mahamid J, Sharir A, Addadi L, Weiner S. Amorphous calcium phosphate is a major component of the forming fin bones of zebrafish: Indications for an amorphous precursor phase. Proc. Natl. Acad. Sci. U S A. 2008; 105:12748–12753. [PubMed: 18753619]

Manoharan R, Baraga JJ, Rava RP, Dasari RR, Fitzmaurice M, Feld MS. Biochemical analysis and mapping of atherosclerotic human artery using FT-IR microspectroscopy. Atherosclerosis. 1993; 103:181–193. [PubMed: 8292094]

Mendelsohn G, Bulkley BH, Hutchins GM. Cardiovascular manifestations of pseudoxanthoma elasticum. Arch. Pathol. Lab. Med. 1978; 102:298–302. [PubMed: 580722]

Neldner KH. Pseudoxanthoma elasticum. Clin. Dermatol. 1988; 6:1–159. [PubMed: 3359381]

Pachman LM, Boskey AL. Clinical manifestations and pathogenesis of hydroxyapatite crystal deposition in juvenile dermatomyositis. Curr. Rheumatol. Rep. 2006; 8:236–243. [PubMed: 16901083]

Pai AS, Giachelli CM. Matrix modelling in vascular calcifiction associated with chronic kidney disease. JASN. 2010; 21:1637–1640. [PubMed: 20798261]

Pleshko N, Boskey A, Mendelsohn R. Novel infrared spectroscopic method for the determination of crystallinity of hydroxyapatite minerals. Biophys J. 1991; 60:786–793. [PubMed: 1660314]

Sauer GR, Wuthier RE. Fourier transform infrared characterization of mineral phases formed during induction of mineralization by collagenase-released matrix vesicles *in vitro*. J. Biol. Chem. 1988; 263:13718–13724. [PubMed: 2843533]

Sauer GR, Zunic WB, Durig JR, Wuthier RE. Fourier transform raman spectroscopy of synthetic and biological calcium phosphates. Calcif. Tissue Int. 1994; 54:414–420. [PubMed: 8062160]

Thouverey C, Bechkoff G, Pikula S, Buchet R. Inorganic pyrophosphate as a regulator of hydroxyapatite or calcium pyrophosphate dihydrate mineral deposition by matrix vesicles. Osteoarthritis Cartilage. 2009; 17:64–72. [PubMed: 18603452]

Tomazic BB, Brown WE, Schoen FJ. Physicochemical properties of calcific deposits isolated from porcine bioprosthetic heart valves removed from patients following 2–13 years function. J. Biomed. Mater. Res. 1994; 28:35–47. [PubMed: 8126027]

Uitto J, Li Q, Jiang Q. Pseudoxanthoma elasticum: Molecular genetics and putative pathomechanisms. J. Invest.Dermatol. 2010; 130:661–670. [PubMed: 20032990]

Uitto J, Bercovitch L, Terry SF, Terry P. Pseudoxanthoma elasticum: Progress in diagnostics and research towards treatment. Summary of the 2010 PXE International Research Meeting. Am. J. Med. Genet. Part A. 2011; 155:1517–1526. [PubMed: 21671388]

Wentrup-Byrne E, Armstrong CA, Armstrong RS, Collins BM. Fourier transform raman microscopic mapping of the molecular components in a human tooth. J. Raman Spectrosc. 1997; 28:151–158.

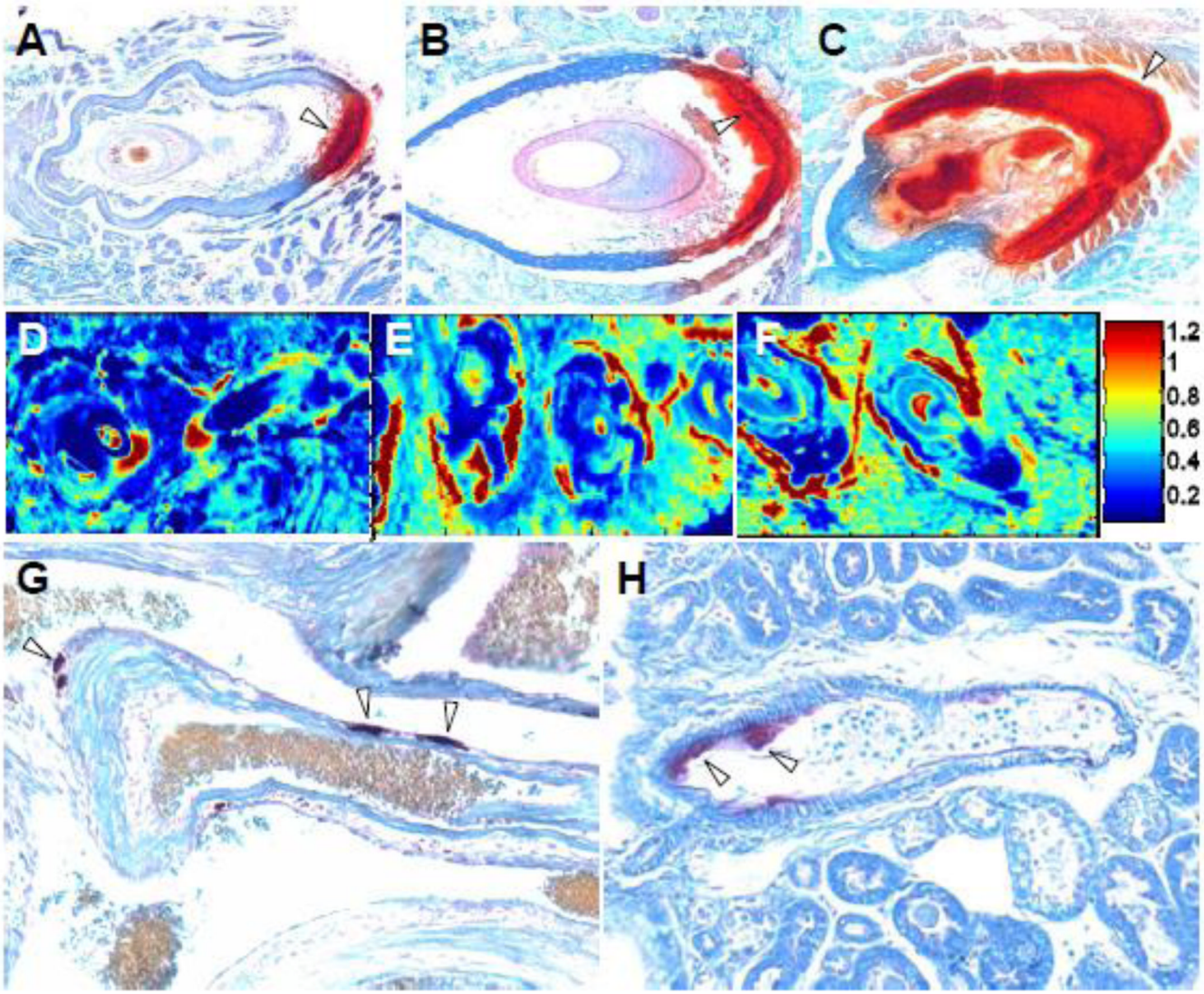

Figure 1.

Ectopic mineralization of the connective tissue capsule surrounding the vibrissae (A–C), and blood vessels in heart (G) and kidney (H), and FT-IRIS images of representative vibrissae samples from mice of different ages, based on the ratio of mineral to matrix peak heights at 1024 and 1660 cm^{-1}. Tissues were isolated from *Abcc6*$^{-/-}$ mice and processed for staining with Alizarin Red. Note the mineralization was indicated with open arrowheads. Note the progressive mineralization in the connective tissue capsule surrounding the vibrissae in 3 months (A,D), 6 months (B,E), and 24 month old mice (C,F), as well as mineralization in the blood vessels of heart and kidney at 24 months of age (G,H). The color scale represents the ratio of the heights of the absorbance bands of mineral to matrix where red indicates the highest and dark blue indicates the lowest.

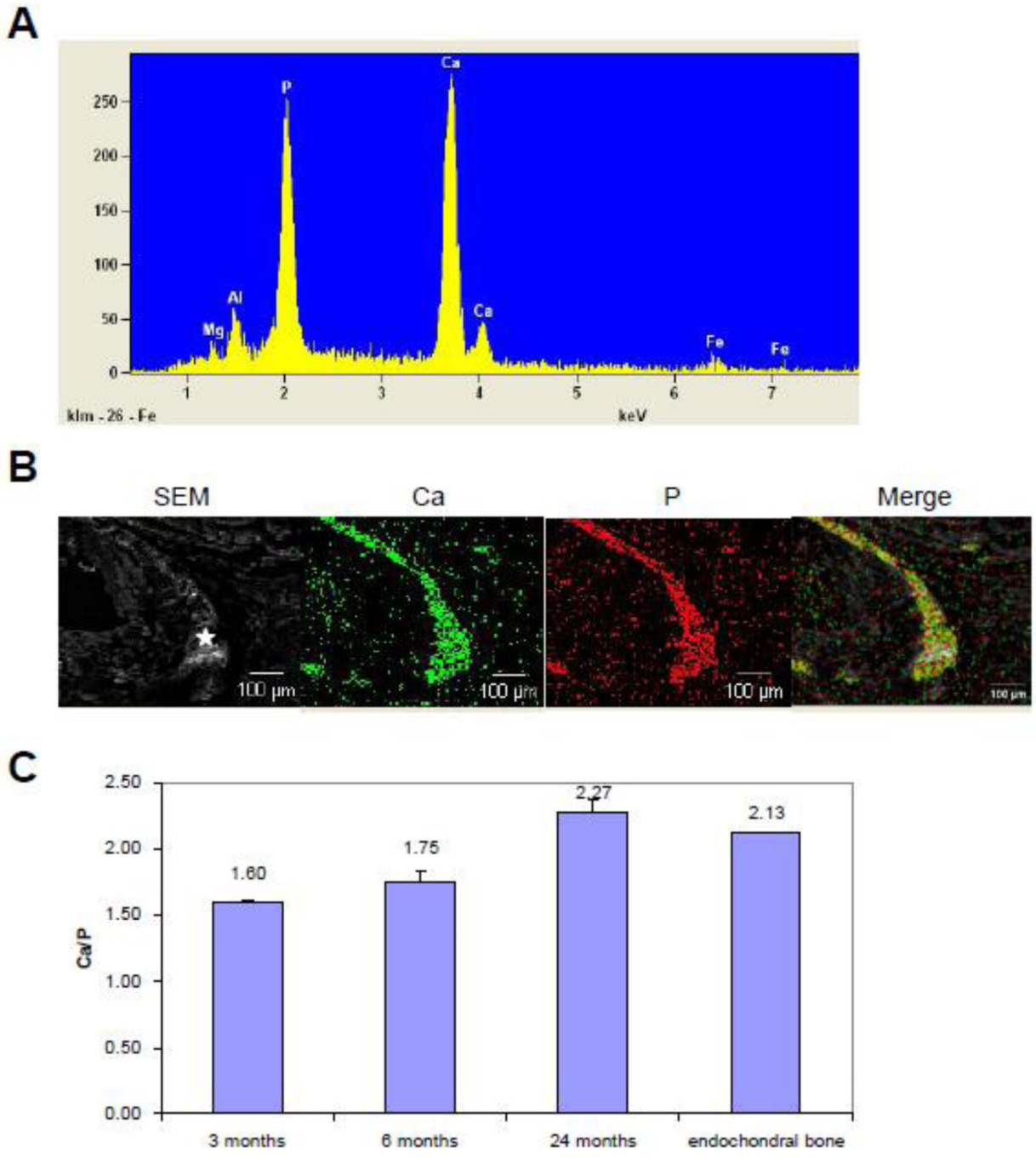

Figure 2.

Characterization of the mineral deposits by EDAX (A), and topographic mapping (B), and the relative content of calcium and phosphate (C). The results indicated dominant peaks corresponding to calcium and phosphate (A), and these ions co-localize in the mineralized connective tissue capsule (B). The ratio of calcium/phosphate increases from 3 months to 24 months old mice, the latter values approximating those measured in endochondral bone (C).

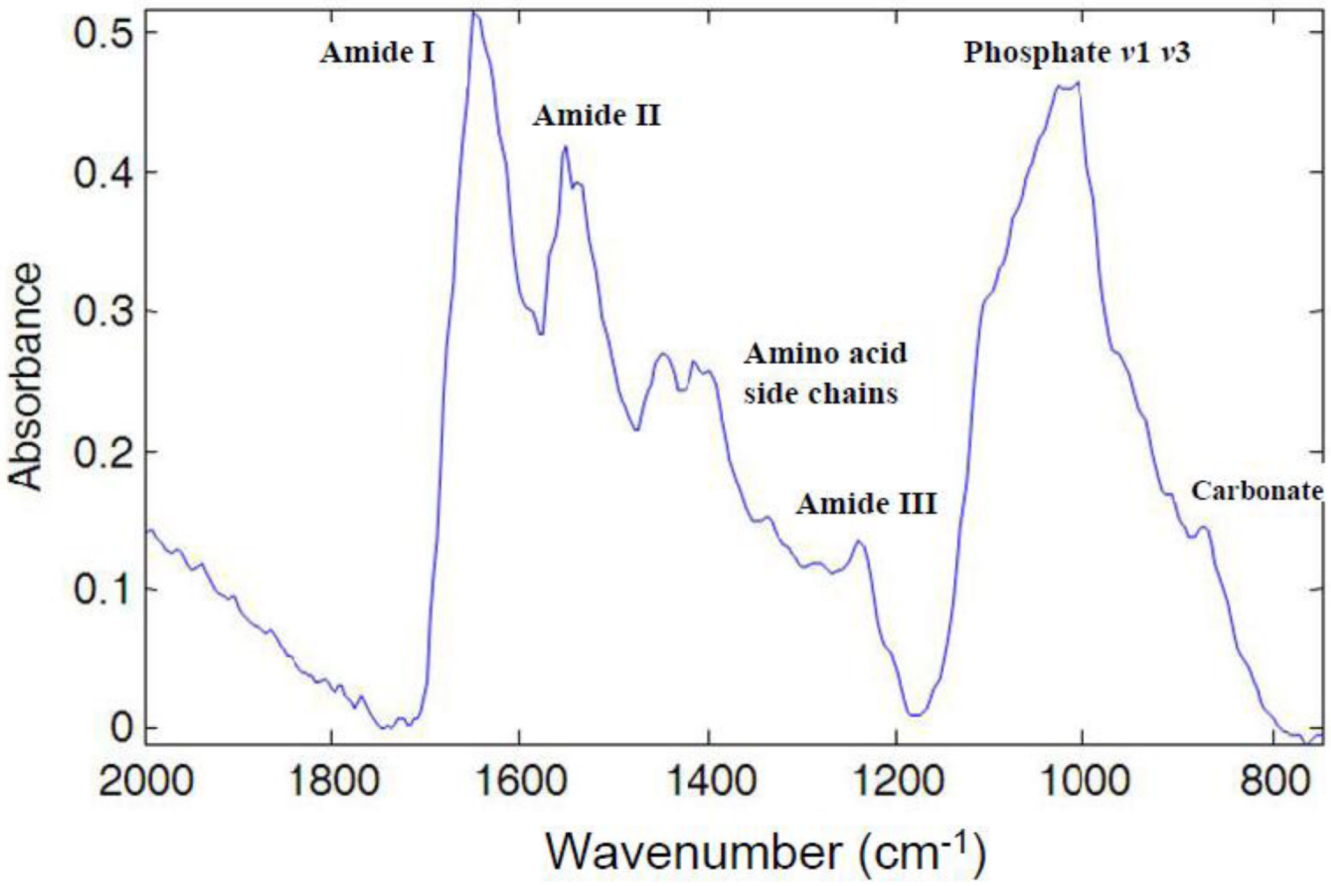

Figure 3.

Illustration of a typical FT-IRIS spectrum of mineralized vibrissae. The bands associated with the vibrations of organic bonds from proteins are shown as amide I (C=O stretch) centered at 1650 cm^{-1}, amide II (C-N stretch and N-H in-plane bending mode) centered at 1550cm^{-1}, amino acid side chain vibrations due to C-H bending motions (overlapping bands 1500–1360 cm^{-1}) and amide III combination band centered around 1250 cm^{-1}, and absorbances from carbonated calcium phosphates as phosphate ν1, ν3 (1200–900 cm^{-1}), and carbonate ν2 (890–840 cm^{-1}).

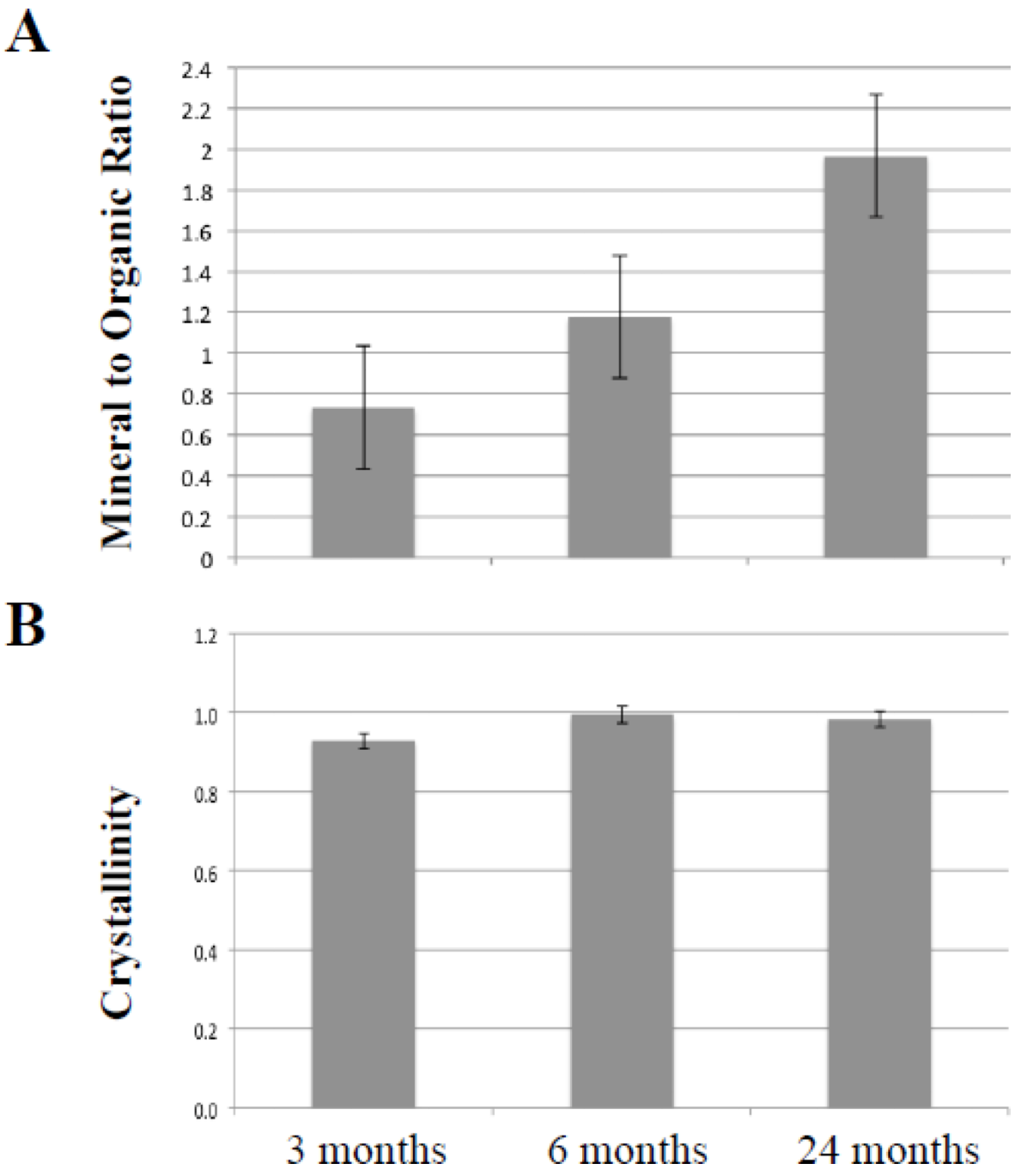

Figure 4.

A. Peak height ratios of the highest absorbance associated with the mineral phase to the absorbance associated with the organic matrix (amide I) in mineral deposits in the connective tissue sheath of vibrissae. The values are mean ± S.E., n = 6–7 per group. B. Peak height ratios of the absorbance at 1030 cm^{-1} and 1020 cm^{-1} representing the mineral crystallinity. The values are ± S.E. from 3–9 determinations per group.

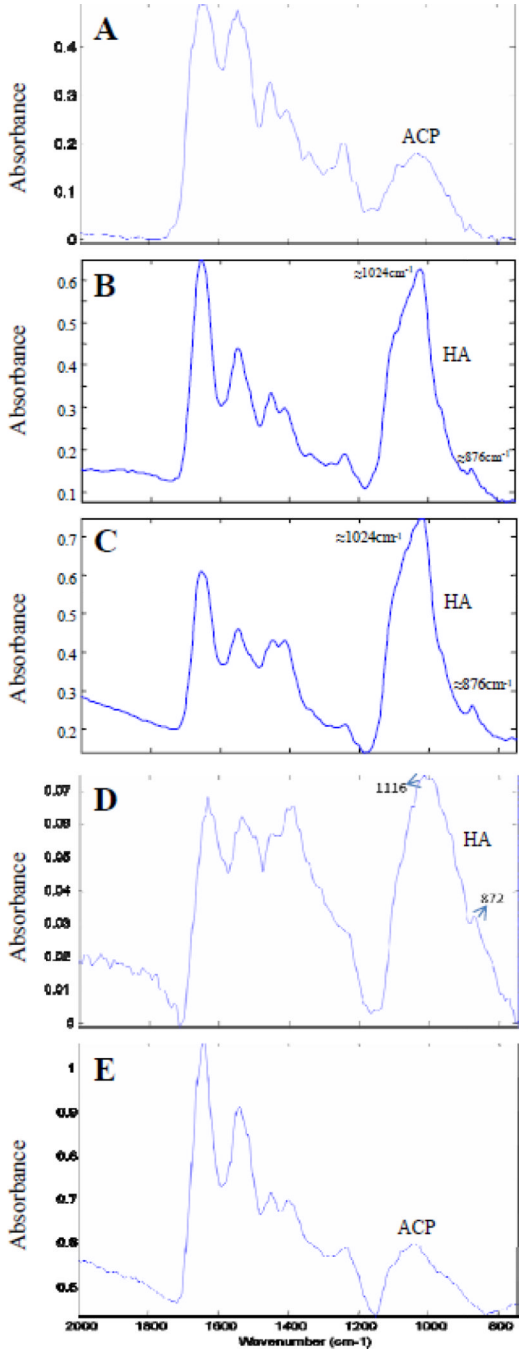

Figure 5.

Representative FT-IRIS spectra from the mineralized region of tissues from *Abcc6*$^{-/-}$ mice of varying ages. A. Three months, vibrissae; spectral absorbance typical of amorphous calcium phosphate (ACP). B. Six months, vibrissae; spectral absorbance typical of poorly crystalline hydroxyapatite (HA). C. Twenty four months vibrissae; spectral absorbance typical of poorly crystalline HA. D. Twenty four months, blood vessels in heart; spectral absorbance typical of poorly crystalline HA. E. Twenty four months, blood vessels in kidney; spectral absorbance typical of amorphous calcium phosphate (ACP).